Sustainable Marine Structures
https://ojs.nassg.org/index.php/sms

ARTICLE

Analysis of Wave Added Drag and Motion Response of Mid-high-speed Ship against Waves

Jing Wang[1*] Yu Zhou[2]

1. China Institute of Marine Technology and Economy, Beijing, 100081, China
2. Jiangsu Shipping College, Nantong, Jiangsu, 226010, China

ARTICLE INFO

Article history
Received: 7 January 2023
Revised: 3 February 2023
Accepted: 27 February 2023
Published Online: 1 March 2023

Keywords:
CFD method
Wave added resistance
Motion response
Numerical pool
Numerical simulation

ABSTRACT

In order to accurately predict the on-wave resistance and responses to hull motions of ships in actual sea conditions, the k-ε method of the RNG model is adopted on the basis of the unsteady RANS method. The two-formula turbulence model deals with the viscous flow, the VOF method captures the free surface, the velocity boundary method makes waves, the artificial damping method is used to eliminate waves, and the nested grid technology is used to deal with the motion response of ships on waves. Combined with the 6-DOF motion formula, a three-dimensional numerical wave cell for regular waves is established. For one example, taking a KCS Container ship and fishing boat sailing at a mid-high-speed, the increase of wave resistance and motion response at different wavelengths are analyzed, and the simulation results are compared with the experimental value, the content of strip theory in potential flow theory and the panel method to prove the reliability of CFD method in predicting ship motion.

1. Introduction

In the actual navigation process, the ship will be affected by waves of different degrees and some movement phenomena, such as heave and pitch. These motions will not only increase the resistance of the ship and reduce the propulsion efficiency, but also affect the normal operation of the equipment on the ship and the working efficiency of the crew, and even cause the ship to capsize. Therefore, accurate prediction of the motion performance of the hull is very vital for ship design. Therefore, the study of ship motion characteristics in waves has become a current hot spot in academic research [1]. The traditional method of studying ship motion performance is based on potential flow theory and model tests. The theory based on potential flow has been widely used for its convenience and rapidity. Particularly in the initial design stage of a ship, in order to quickly obtain the motion performance of ships, it has been favored by ship

*Corresponding Author:
Jing Wang,
China Institute of Marine Technology and Economy, Beijing, 100081, China;
Email: jingwang_erccsic@163.com

DOI: http://dx.doi.org/10.36956/sms.v5i1.804

designers. However, because there is a big error between the numerical simulation results and the theoretical calculation results, it is a difficult to accurate prediction of nonlinear results such as the increase of ship motion amplitude, wave breaking and waves on the deck [2]. Therefore, it is very important to obtain more flow field information at the stage of ship detailed design. Although the calculation results of the model experiment are accurate, due to a large number of manpower and costs, it cannot meet the requirements of the current fierce market competition for the rapid acquisition of new ship types. In recent years, with the rapid development of computer technology and mathematical knowledge, using CFD technology to predict wave resistance and motion performance has become a reality. CFD method not only considers the viscous effect, but also fully considers the nonlinear effect, so it has been widely used. Many research results have been published at home and abroad to predict wave resistance and motion performance using CFD. In foreign countries, for RANS formula, is solved by Orihara and Miyata [3] through the finite volume method, and used the overlapping grid technology to simulate and calculate the wave resistance and motion of container ships in regular waves. The numerical value of the DTMB5512 ship-type large-amplitude motion is calculated and summarized by Carrica and Wilson [4], which is at medium and high speed, using overlapping grid technology. Tezdogan and Kemal Demirel [5] and others evaluated the resistance and motion of container ships at low speeds following the waves using the unsteady RANS method. In China, the CFD solver name-Foam-SJTU independently developed by Shen Zhirong [6] team based on the open-source code OpenFOAM can well predict the motion performance of ships and marine engineering and has been verified by experiments. Zhao Invention [7] and others developed a CFD hydrodynamic performance calculation system for ships based on the RANS method of overlapping grids, which can well simulate the resistance and response of ship motion. Shi Bowen [8] and others set up a three-dimensional numerical simulation wave-making water channel based on the viscosity principle. In this way, the performance of ship navigation in irregular waves is simulated. However, the resistance and response of different ship types moving on the waves are different. The KCS Container ship and fishing boat are mid-high-speed ships, and there are few detailed studies on wave resistance and motion response. Based on the above conditions and experience, this paper numerically simulates the motion of fishing boats in waves in a six-degree-of-freedom regular wave numerical pool based on the unsteady RANS method, calculates the wave resistance and motion response, and verifies the reliability of this method by numerical calculation. The numerical calculation methods here include the strip theory method and panel method. The research results of this paper can provide technical support for the design and optimization of similar ships.

2. Basic Theory of CFD

The formulas followed in the calculation domain of the whole simulated pool are the continuity formula and N-S formula, and the turbulence model adopts the k method of RNG-ε. In the model, capture free liquid surface by multiphase flow model method. And the wave is generated at the given wave velocity at that border of the speed inlet, and a factitious damping setting is added wave pool exit area for wave attenuation.

2.1 Control Formula

$$\frac{\partial \rho}{\partial t}+\frac{\partial(\rho u_x)}{\partial x}+\frac{\partial(\rho u_y)}{\partial y}+\frac{\partial(\rho u_z)}{\partial z}=0 \quad (1)\ [9]$$

$$\rho\frac{\partial \overline{u_i}}{\partial t}+\rho\overline{u_j}\frac{\partial \overline{u_i}}{\partial x_j}=-\frac{\partial \overline{p}}{\partial x_i}+\mu\frac{\partial^2 \overline{u_i}}{\partial x_j \partial x_j}-\rho\frac{\partial \overline{u_i' u_j'}}{\partial x_j}+\rho\overline{f_i} \quad (2)$$

where, u_x, u_y, u_z are velocity components in x, y and z directions; t is time; ρ is the quality density of fluid; $\overline{u_i}$ is Reynolds mean velocity; $\rho\overline{u_i' u_j'}$ Reynolds stress.

2.2 Turbulence Model

The turbulence model adopts the k method of RNG-ε. In the model, the turbulent energy formula and energy consumption formula are in the following form [10]:

$$\frac{\partial(\rho k)}{\partial t}+\frac{\partial(\rho k u_i)}{\partial x_i}-\frac{\partial}{\partial x_j}[(\alpha_k \mu_{eff})\frac{\partial k}{\partial x_j}]=G_k+G_b-\rho\varepsilon-Y_M \quad (3)$$

$$\frac{\partial(\rho\varepsilon)}{\partial t}+\frac{\partial(\rho\varepsilon u_i)}{\partial x_i}-\frac{\partial}{\partial x_j}[(\alpha_\varepsilon \mu_{eff})\frac{\partial \varepsilon}{\partial x_j}]=c_{\varepsilon 1}\frac{\varepsilon}{k}(G_k+c_{\varepsilon 3}G_b)-c_{\varepsilon 2}\rho\frac{\varepsilon^2}{k}-R \quad (4)$$

where, $\mu_{eff}=\mu+\rho C_\mu\frac{k^2}{\varepsilon}$; α_k, α_ε are the reciprocal of turbulence kinetic energy's effective prandtl number and turbulent dissipation rate.

2.3 Free Face Snap

Under the condition of keeping the Euler grid unchanged, the interface between the ship and the water surface is captured by the free following of the hull surface, which is called the VOF method [11]. It can be used to simulate the multi-flow model by finding the solution of the momentum formula and volume fractions of a fluid or fluids. In any control volume, the sum of the volume fractions of all phases must be 1. For each qth phase, the formula is:

$$\frac{\partial a_q}{\partial t}+\frac{\partial (ua_q)}{\partial x}+\frac{\partial (va_q)}{\partial y}+\frac{\partial (wa_q)}{\partial z}=0 \tag{5}$$

$$\frac{\partial \alpha_q}{\partial t}+v_q*\nabla \alpha_q=\frac{S_{\alpha_q}}{\rho_q}+\frac{1}{\rho_q}\sum_{p=1}^{n}(\dot{m}_{pq}-\dot{m}_{qp}) \tag{6}$$

where, a_1 and a_2 are the volume fractions of water and air respectively, and aq = 0.5, which is the limiting surface between water and air; q = 0, which represents that the entire computing domain is water; q = 1, which represents that th entire computing domain is air.

2.4 Wave Making and Wave Absorption

This wave-making adopts the velocity boundary method, which makes waves by giving the wave velocity at the boundary of the velocity entrance [12]. Compared with the physical test pool, It has high economic value, convenient operation, high calculation accuracy and slow attenuation. At the same time, this method is easier to give a fixed velocity of the vessel at the entrance boundary, which can avoid difficulties brought by moving the boundary, which is another advantage compared with the simulated physical method.

The wave surface formula is:

$$\eta = a\cos(kx-\omega_e t) \tag{7}$$

The speed influences are as follows:

$$u = a\omega_0 e^{kz}\cos(kx-\omega_e t)+U \tag{8}$$

$$w = a\omega_0 e^{kz}\sin(kx-\omega_e t) \tag{9}$$

where, a is wave amplitude. K = 2π/λ determine, which is called wave number. ω_0 is natural frequency of wave, $\omega_0=\sqrt{2\pi g/\lambda}$. ω_e can be calculated by formula: $\omega_e = \omega_0+kU$, which is called the frequency of a wave as measured by its relative velocity and wavelength. This equation shows that ω_e varies with the change of the velocity of the vessel U.

The expression of artificial damping coefficient μ is as follows:

$$\mu £(x,z)=\alpha(\frac{x-x_f}{x_a-x_f})^2(\frac{z_d-z}{z_d-z_u}) \tag{10}$$

where, $x_f \le x \le x_a$ (f and a are the two endpoints of the resistance region in the X direction, separately); $z_d \le z \le z_u$ (d and u are the bottom along the y direction and the intersection of water and air separately); α is the damping control parameter.

2.5 DOF Equation of Motion

When establishing the ship motion formula, two reference coordinate systems are established. One is the fixed coordinate system OoXoYoZo, which is fixed on the earth. The other is the ship moving coordinate system GXYZ, which is fixed on the ship [13]. The origin of the moving coordinate system is located at the center of gravity G of the ship, where Gx, Gy and Gz are the intersection lines of the longitudinal section, the transverse section and the horizontal liquid level passing through the center of gravity G, respectively, and the downward direction of the Z axis is positive[14].

$$\frac{\mathrm{dB}}{\mathrm{dt}}+\Omega\times B=F \tag{11}$$

$$\frac{\mathrm{dK}}{\mathrm{dt}}+\Omega\times K+U\times B=M \tag{12}$$

where, Ω is the angular velocity, B is the ship's moment, F is the additional force, U is the ship's speed, K is the moment of momentum, and M is the sum moment.

3. Verification of Numerical Calculation Method

3.1 Main Dimensions of KCS Ship

KCS ship type is a medium and high-speed container ship with complete experimental data, and is a general hull for design and experiment[15]. In this paper, the additional wave resistance, heave and pitch of the KCS ship are calculated. The correctness of the CFD numerical calculation method is verified by comparing it with the experimental values. The three-dimensional model of the KCS ship is shown in Figure 1, and the main dimensions are shown in Table 1.

Figure 1. Geometric model of KCS ship form.

Table 1. Main dimensions and ship form parameters of KCS ship model and real ship.

Parameter	Unit	Ship model	Full-scale ship
Scale ratio	-	52.55	1
Length between perpendiculars (L_{PP})	m	4.3767	230
Ship width (B)	m	0.611	32.2
Draft (d)	m	0.205	10.8
Wet surface area (S)	m^2	3.436	9424
Square coefficient (C_B)	-	0.65	0.65
Froude number (Fr)	-	0.26	0.26

3.2 Computational Domain and Calculation Condition

In this paper, a three-dimensional numerical flume is established to simulate the KCS ship form. The size of the calculation area is: the distance from the entrance of the calculation area to the bow is 1.33 L, the depth of the calculation area in the Z direction is 6 L, the width in the Y direction is 2 L, and the distance from the stern to the exit of the calculation area is 4 L (where L is the length between the vertical lines of the hull, in m). The lower part of the free surface is water and the upper part is air. The boundary conditions include velocity inlet, pressure outlet and symmetrical boundary conditions. In this paper, the wavelength length ratio λ/L=0.75~2.00 is the calculation condition, and the motion response of KCS ship type at different wavelengths is analyzed by changing the wavelength to conduct a mathematical simulation.

3.3 Meshing

In CFD calculation, mesh division has a key impact on the calculation results and calculation speed. In this paper, the overlapping grid technology is used to divide the hull and computing domain, as shown in Figure 2 and Figure 3. The hull parts (such as the bow and stern) with sharp curvature changes are meshed to ensure that their geometric shape is basically unchanged. In addition, the free surface part that has a great impact on the calculation results has been densified to ensure that there are 80 grids in the wavelength range and 40 grids in the wave height range, and the final number of grids is about 2.4 million.

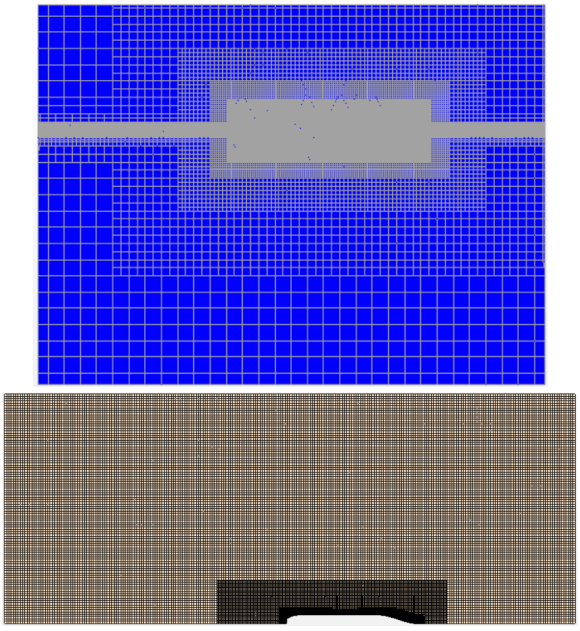

Figure 2. Calculation domain and free surface meshing.

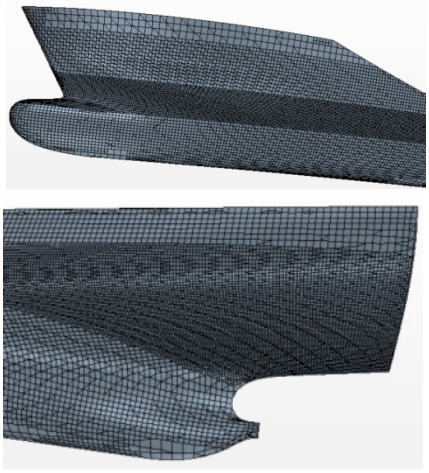

Figure 3. Hull surface meshing.

3.4 Calculation Results

3.4.1 Grid Uncertainty Analysis

The accuracy of mesh density is very important for the accuracy of results. Therefore, before numerical simulation based on the CFD method, it is necessary to use test data to analyze the uncertainty of grid division. In this paper, three sets of grid settings are set. The main difference is the basic size of the mesh. According to the grid density, the results of the three examples can be divided into S1 (coarse), S2 (medium) and S3 (fine), as shown in Figure 4.

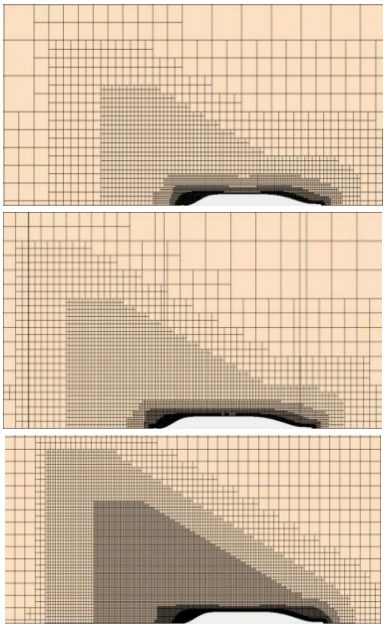

Figure 4. Grid division of three groups of density.

According to ITTC (2002), the three sets of grid refiner base size ratio ri (uniform parameter refinement ratio) are

set to 1.414. The uncertainty is calculated as follows:

$$R_i = \frac{\varepsilon_{i,21}}{\varepsilon_{i,32}} \tag{13}$$

$$\delta^{*(1)}_{RE_{i,1}} = \frac{\varepsilon_{i,21}}{r_i^{p_i} - 1} \tag{14}$$

$$p_i = \frac{In(\varepsilon_{i,32} / \varepsilon_{i,21})}{In(r_i)} \tag{15}$$

$$\delta^*_{i,1} = C_i \delta^*_{RE_{i,1}} = C_i \frac{\varepsilon_{i,21}}{r_i^{p_i} - 1} \tag{16}$$

$$C_i = \frac{r_i^{p_i} - 1}{r_i^{p_{iest}} - 1} \tag{17}$$

In the formula: C_i is the Correction Factor, p_{iest} is the estimate of the first precision limit order, because the interval size is zero and reaches the asymptotic range, therefore $C_i \rightarrow 1$, $p_{iest} = 2$.

When C_i is much less than or greater than 1,

$$U_i = (|C_i| + |1 - C_i|)\left|\delta^*_{RE_{i,1}}\right|, \quad |1 - C_i| > 0.125 \tag{18}$$

$$E = D - S_1 \tag{19}$$

$$U_V \approx \sqrt{U_D^2 + U_i^2} \tag{20}$$

$U_D = 2\%$ D, D is the experimental value.

$$S_C = S_1 - \delta^*_{i,1} \tag{21}$$

$$E_C = D - S_C \tag{22}$$

$$U_{i_C} = |1 - C_i|\left|\delta^*_{RE_{i,1}}\right|, \quad |1 - C_i| > 0.25 \tag{23}$$

$$U_{V_C} \approx \sqrt{U_D^2 + U_{i_C}^2} \tag{24}$$

The total drag coefficients in the uncertainty analysis are extrapolated to full scale following ITTC 78. (Details can be referred to 7.5-02-03-01.4). The present results are valid when $|E| < U_V$ and $|E_C| < U_{VC}$. In this paper, the uncertainty of the total resistance coefficient of the KCS ship is analyzed. The results are shown in Table 2.

Table 2. Results of uncertainty analysis.

CFD CTs (10–3)			**EFD CTs (10–3)**			
S1	S2	S3	D	ri	Ri	pi
3.96	3.58	3.63	3.67	1.414	0.712	0.98
$\delta^*_{RE}(1)$(%D)	E(%D)	U_V(%D)	E_C(%D)	U_{VC}(%D)	S_C (10-3)	U_D(%D)
4.703E-05	8.6E-05	1.2 E-04	3.897E-05	1.014E-04	3.672	0.404
	S_1		S_2		S_3	
Number of the grids	1600000		2400000		2850000	
Base size	0.08 m		0.06 m		0.04 m	

3.4.2 Comparison of CFD Calculated Value and Test Value

Figure 5, Figure 6 and Figure 7 are the comparisons of CFD simulation results and experimental values of the heave transfer function, pitch transfer function and wave additional resistance coefficient. It can be seen from the figure that the CFD calculation result is close to the experimental value, and the error is within 3%, meeting the engineering calculation accuracy requirements. Figure 8 shows the free surface wave waveform of the KCS ship type, showing the obvious shape of the Kelvin wave system. Figure 9 shows the hull surface pressure of the KCS ship type, with obvious slamming at the bow.

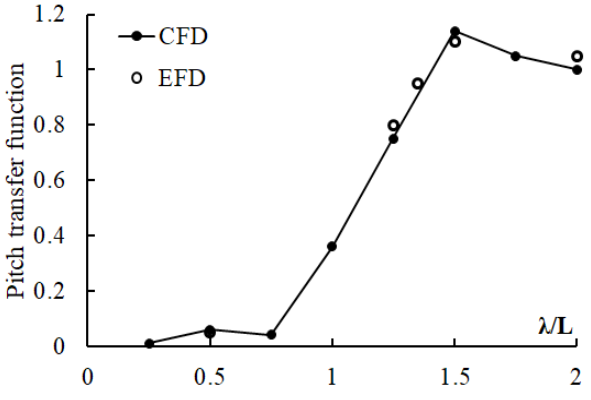

Figure 5. Heave transfer coefficient.

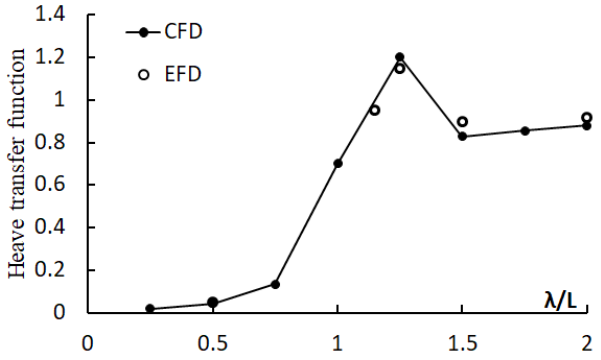

Figure 6. Pitch transfer function.

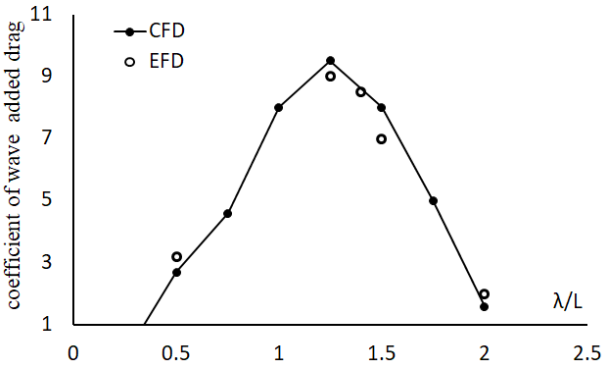

Figure 7. Wave drag coefficient.

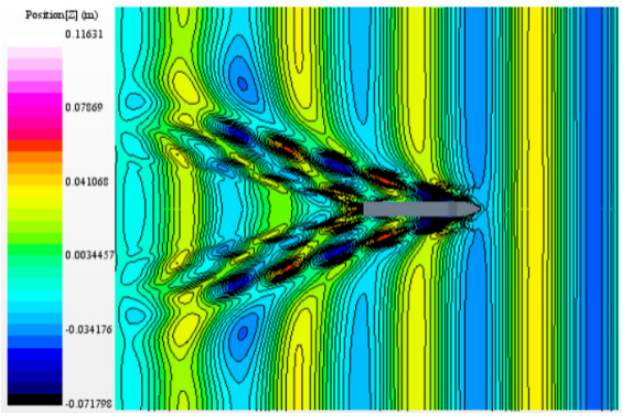

Figure 8. Waveform of interface between water and air (Fn = 0.26, λ/L = 1.0).

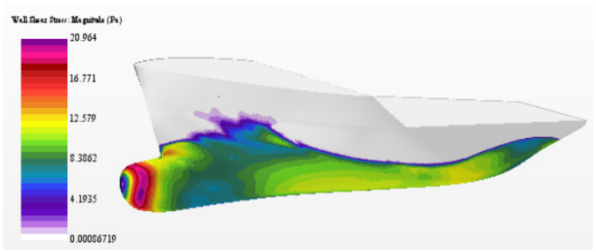

Figure 9. Change of hull shear stress over a period of time (Fn = 0.26, λ/L = 1.0).

4. Calculation of Motion Response of Fishing Boat

The wave resistance and body responses of high-speed fishing boats sailing in waves are calculated. Figure 10 shows the fishing boat's geometric model. And the main dimensions and hull form parameters are shown in Table 3.

Figure 10. Geometric model of the fishing vessel.

Table 3. The fishing vessel's main dimensions and hull form parameters.

Parameter	Full-scale ship	Model	Unit
Length between perpendiculars (L_{pp})	34.5	4.8	m
Draft (d)	2.5	0.35	m
Moulded width (B)	7.6	1.06	m
Square coefficient (C_B)	0.597	0.597	-
Displacement (Δ)	425	1.45	t
Wet surface area (S)	324	6.27	m^2
Design speed	35	13	kn

4.1 Calculation Domain and Boundary Conditions

According to the symmetry of the hull, it can be assumed that the flow field is also symmetrical in the numerical simulation, and the symmetry plane is the X-Z plane. Considering the parameters such as wavelength, period and wave height of simulated linear waves, taking half of the hull as the calculation domain can effectively improve the calculation speed. Taking the calculation range of 4.5 L×2.0 L×2.5 L (where L is the captain and the unit is m) as the whole calculation domain, that is, the numerical simulation research object. The distance between the bow and the pool entrance is L, and the simulated water depth is 1.5 L. The specific dimensions are shown in Figure 11. The upper part of the computational domain is air and the lower part is water.

The boundary setting of the velocity inlet is applied to the front surface, the upper surface and the lower surface of the numerical simulation wave pool respectively, and the inflow velocity is added to the boundary of the front surface, which is the velocity of the vessel. Attach the pressure outlet parameter to the rear surface. Attach a rigid surface (wall) parameter to the surface of the boat. Finally, the calculation domain is set to be symmetric on the boundary of the middle longitudinal profile and its opposite sides.

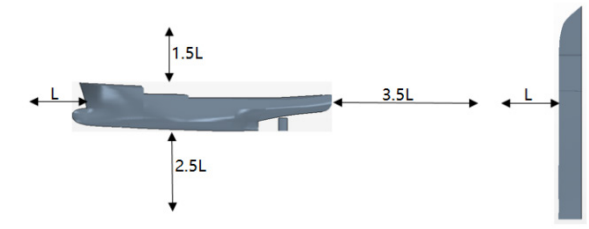

(a)

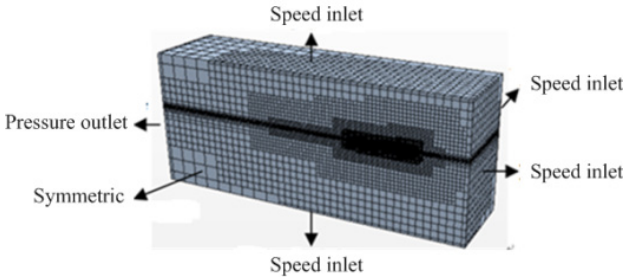

(b)

Figure 11. Calculation domain and boundary conditions.

4.2 Meshing

Meshing is an essential part of the numerical simulation process. If you change the density and form of the grid, it will change the overall simulation time and the judgment of the results. Therefore, only by grasping the effect of the grid can you control the accuracy and reliability of the calculation results. In this paper, the embedded grid technology is applied in the commercial software STAR-CCM+, and static and dynamic grids are established. As to better analyze the ship's trajectory and sway on waves. Among them, static grids are sparsely drawn, and dynamic grids can be densely drawn with encrypted grids. Overlap and background grid junction should be excessive according to a constant ratio. The interface between air and water must be no less than 80 grilles in the wavelength distance and no less than 20 gratings in the peak-to-trough range. Considering the machine configuration and simulation time, the total number of grids finally determined is 1.85 million. Figure 12 shows the grid near the free surface. As can be seen from the figure, the closer to the hull, the dense the grid, and the farther away from the hull, the more sparse the grid. Figure 13 shows the size and shape of the hull surface grid. And grid encryption is needed at the bow and stern.

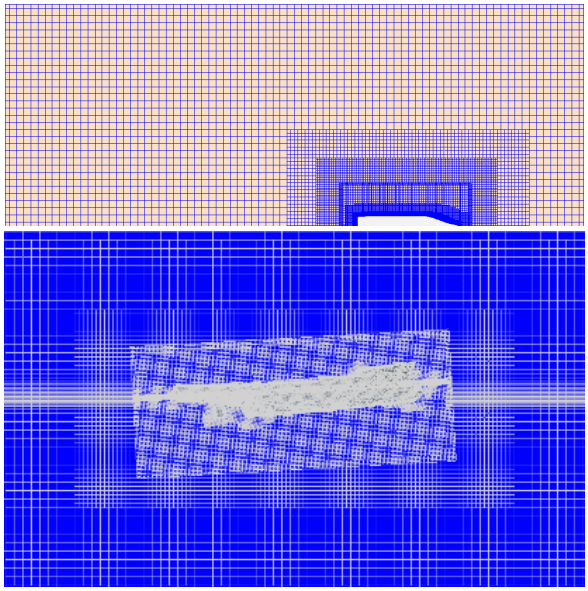

Figure 12. Grid division of free surface and longitudinal section.

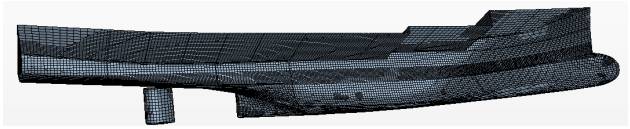

Figure 13. Hull grid division.

4.3 Grid Independence Check

Mesh number has a great impact on the calculation results. The number of grids is too large, which wastes computing resources, is too small, and the results are inaccurate. As a result, it is essential to find a number of grids appropriately. In this paper, five types of grids are calculated respectively, and the calculation grid with less influence on the calculation results due to the increase of grid is obtained. Future calculations are based on this grid. The calculation results are shown in Figure 14.

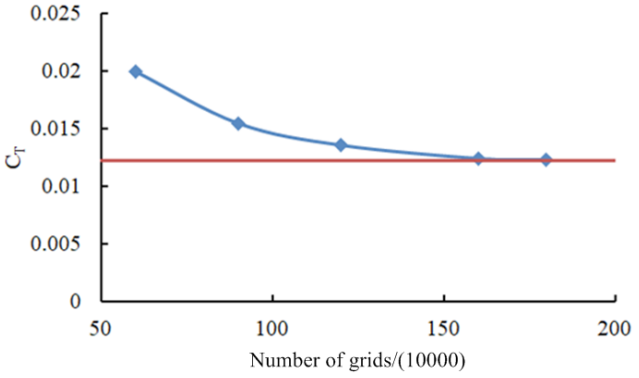

Figure 14. Grid independence.

4.4 Calculation Conditions of Wave Drag Increase

This paper mainly simulates the motion law of fishing boats under different wavelength length ratios and different wave steepness. Take the wavelength to length ratio: λ/L=0.75, λ/L=1.00, λ/L=1.25, λ/L=0.50, λ/L=7.75, λ/L=2.00; and wave steepness: 0.0175, 0.035, 0.0775, 0.0875 as the calculation conditions. The volume fraction of fishing boats is shown in Figure 15.

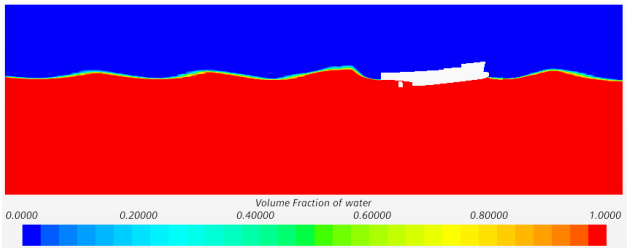

Figure 15. Volume fraction of the fishing vessel.

4.5 Analysis of Simulation Results

Figure 16 shows the relationship between the shear stresses received by the fishing boat hull over a period of time. It can be seen from the figure that the hull shear stress will change continuously with the wave peak and its steepness, especially the bow will bear huge shear stress in 1/4-1/2 cycle, because the bow is located at the wave peak position at this time, and there will be phenomena such as burying the bow or wave on the deck.

Figure 17 shows the changing relationship of the free surface of the hull over a period of time. It can be seen from the figure that the change of draught at the bow and both sides of the hull can clearly show severe heave movements and pitch movements. In addition, waves appeared on the deck. The severe pitching motion may cause the bulbous nose to constantly enter and exit the water surface, resulting in a loud bang on the head, which will worsen the seakeeping of the ship.

Figure 18, Figure 19 and Figure 20 are the comparisons of the CFD simulation results of the heave, pitch transfer function and wave resistance coefficient of fishing vessels using the slice theory and the panel method respectively. It can be seen from the figure that the calculation curve trend of the three methods is basically the same, and they can well predict the relationship between heave, pitch and wave resistance with the increase of wavelength-to-length ratio. The accuracy of the CFD calculation method has been confirmed by engineering practice, so the CFD simulation results should still prevail in the absence of test values. In addition, the heaving and pitching relationships of the fishing vessel under different wave steepness are also studied. As can be seen from Figure 21, the heave of the ship increases slowly and gradually with the increase of wave steepness. In contrast, the pitching of a ship increases rapidly and gradually with the steep waves.

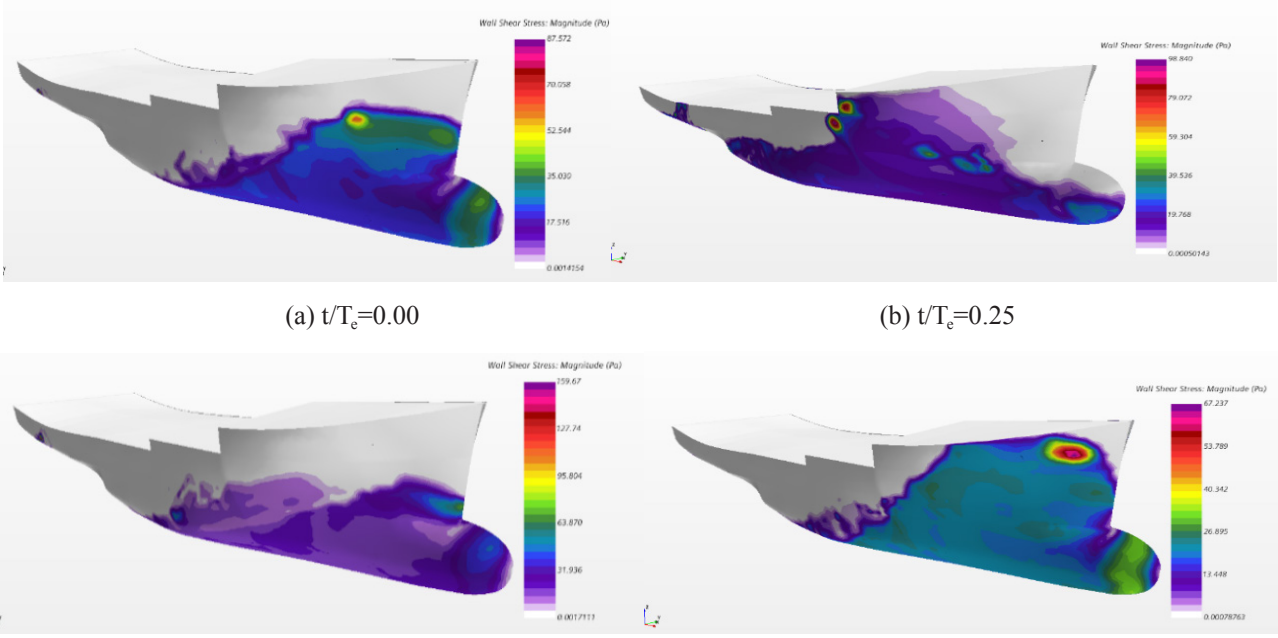

(a) t/T_e=0.00 (b) t/T_e=0.25

(c) t/T_e=0.50 (d) t/T_e=0.75

Figure 16. Change of hull shear stress over a period of time (Fn = 0.28, λ/L = 1.0).

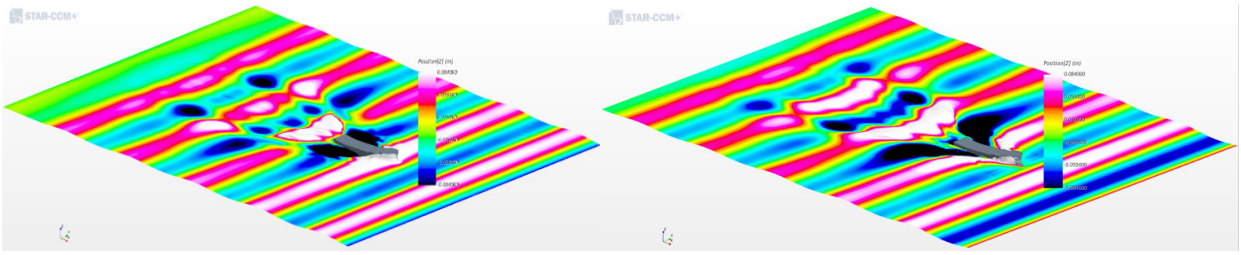

(a) t/T_e=0.00 (b) t/T_e=0.25

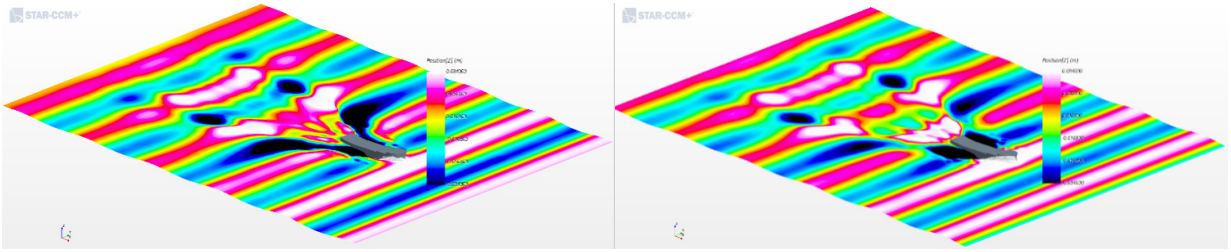

(c) t/T_e=0.50 (d) t/T_e=0.75

Figure 17. Waveform of interface between water and air in one cycle (Fn = 0.28, λ/L = 1.0).

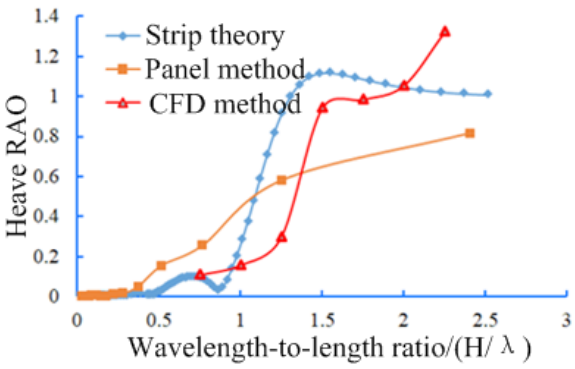

Figure 18. The heave transfer coefficient.

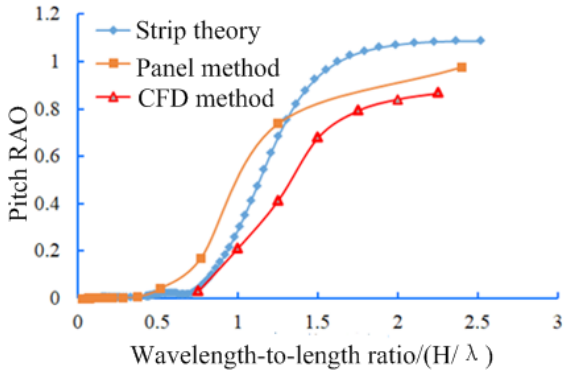

Figure 19. The pitch transfer function.

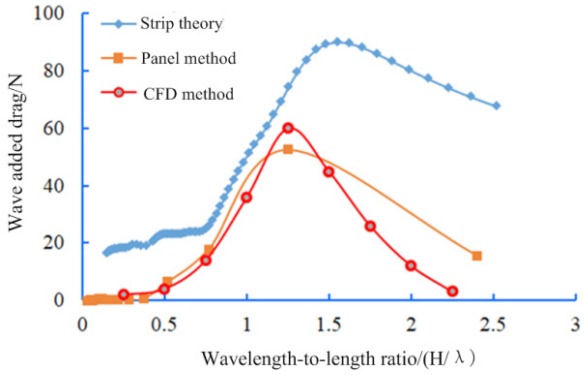

Figure 20. Wave resistance coefficient.

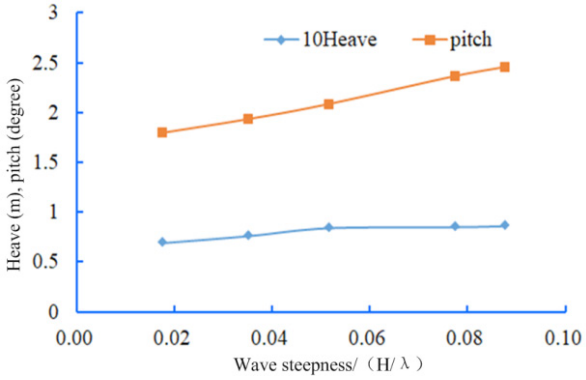

Figure 21. The heaving and pitching values of the fishing vessel under different wave steepness.

5. Conclusions

Based on the CFD method, the commercial CFD software STAR-CCM+ is used to study the resistance and motion response of high-speed fishing boats in waves. The first-order Stokes wave numerical flume is established to simulate the wave resistance, heave and pitch motion response of fishing vessels under the condition of a wavelength length ratio of 0.75 to 2.25. The shape of the Kelvin-free surface wave system is reproduced, and the relationship and reason for the change of the hull surface shear stress are analyzed. Finally, the results of CFD numerical simulation are compared with those of strip theory and panel method, which shows that the CFD method has advantages in simulating ship motion and resistance.

Conflict of Interest

There is no conflict of interest.

References

[1] Zakerdoost, H., Ghassemi, H., Ghiasi, M., 2013. Ship hull form optimization by evolutionary algorithm in order to diminish the drag. Journal of Marine Science and Application. (12), 170-179.

[2] Serani, A., 2016. Hybrid global/local optimization methods in simulation-based shape design [PhD thesis]. Roman: Universit`a degli studi Roma Tre.

[3] Zhao, F., Li, Sh.Zh., Yang, L., 2010. Review of research progress in ship form optimization design based on CFD. Ship Mechanics. 14(7), 812-821.

[4] Orihara, H., Miyata, H., 2003. Evaluation of added resistance in regular incident waves by computational fluid dynamics motion simulation using an overlapping grid system. Journal of Marine Science and Technology. 8(2), 47-60.

[5] Carrica, P.M., Wulson, R.V., Noack, R.W., et al., 2007. Ship motions using single-phase level set with dynamic overset grids. Computers and Fluids. 36(9), 1415-1433.

[6] Tezdogan, T., Demirel, Y.K., Kellett, P., et al., 2015. Full-scale unsteady RANS CFD simulations of ship behaviour and performance in head seas due to slow steaming. Ocean Engineering. 97, 186-206.

[7] Shen, Zh.R., Ye, H.X., Wan, D.Ch., 2014. URANS simulations of ship motion responses in long-crest irregular waves. Journal of Hydrodynamics. 26(3), 436-446.

[8] Zhao, I., Gao, Ch.J., Xia, Q., 2011. Application of overlapping grids in ship CFD. Ship Mechanics. 15(5), 332-341.

[9] Shi, B.W., Liu, Zh.J., Wu, M., 2014. Numerical simulation of top wave motion in irregular waves of ship model. Ship Mechanics. 18(8), 906-915.

[10] Lin, P., Liu, P.L.F., 1998. A numerical study of breaking waves in the surf zone. Journal of Fluid Mechanics. 24(3), 239-264.

[11] Zhang, Sh.L., Zhang, B.J., Lai, Y.Y., et al., 2017. Computational fluid dynamics based hull form optimization using approximation method. Engineering Applications of Computational Fluid Mechanics. 12(3), 1-8.

[12] Masoudian, M., Pinho, F.T., Kim, K., et al., 2016. A RANS model for heat transfer reduction in viscoelastic turbulent flow. International Journal of Heat & Mass Transfer. 100, 332-346.

[13] Claus, D., Simonsen, J.F., Otzen, S.J., 2013. EFD and CFD for KCS heaving and pitching in regular head Waves. Journal of Marine Science and Technology. 18, 435-459.

[14] Zhang, Sh.L., Zhang, B.J., Lai, Y.Y., et al., 2017. Research on bulbous bow optimization based on the improved PSO algorithm. China Ocean Engineering. 31(4), 487-494.

[15] Maki, A., Umeda, N., Renilson, M., et al., 2010. Analytical formulae for predicting the surf-riding threshold for a ship in following seas. Journal of Marine Science and Technology. 15(3), 218-229.